

This is a repository copy of *KIN7 kinase regulates the vacuolar TPK1 K+ channel during stomatal closure*.

White Rose Research Online URL for this paper:

<https://eprints.whiterose.ac.uk/126750/>

Version: Accepted Version

Article:

Isner, Jean-Charles Eric Francois, Begum, Afroza, Nuehse, Thomas et al. (2 more authors) (2018) KIN7 kinase regulates the vacuolar TPK1 K+ channel during stomatal closure. *Current Biology*. 466-472.e4. ISSN 0960-9822

<https://doi.org/10.1016/j.cub.2017.12.046>

Reuse

This article is distributed under the terms of the Creative Commons Attribution-NonCommercial-NoDerivs (CC BY-NC-ND) licence. This licence only allows you to download this work and share it with others as long as you credit the authors, but you can't change the article in any way or use it commercially. More information and the full terms of the licence here: <https://creativecommons.org/licenses/>

Takedown

If you consider content in White Rose Research Online to be in breach of UK law, please notify us by emailing eprints@whiterose.ac.uk including the URL of the record and the reason for the withdrawal request.

1

2 KIN7 kinase regulates the vacuolar TPK1 K⁺ channel during stomatal
3 closure.

4
5 AUTHORS: Jean Charles Isner¹, Afroza Begum², Thomas Nuehse³, Alistair M
6 Hetherington¹ and Frans J.M. Maathuis²

7
8 Affiliations: ¹) School of Biological Sciences, University of Bristol, Life Sciences Building,
9 24 Tyndall Avenue, Bristol BS8 1TQ, UK,

10 ²) Department of Biology, Wentworth Way, University of York, York, YO10 5DD, UK

11 ³) Faculty of Life Sciences, Michael Smith Building, Oxford Road, Manchester, M13 9PT,
12 UK

13
14 Corresponding author and lead contact: Frans J.M. Maathuis, Department of Biology,
15 University of York, York, YO10 5DD, United Kingdom. Tel: +44-1904-328652, Fax:
16 +44-1904-328505, email: fjm3@york.ac.uk

23 **Summary**

24 Stomata are leaf pores that regulate CO₂ uptake and evapotranspirational water loss. By
25 controlling CO₂ uptake stomata impact on photosynthesis and dry matter accumulation.
26 The regulation of evapotranspiration is equally important because it impacts on nutrient
27 accumulation, leaf cooling and enables the plant to limit water loss during drought [1]. Our
28 work centres on stomatal closure [2-6]. This involves loss of potassium from the guard cell
29 by a two-step process. Salt is released across the plasma membrane via anion channels
30 such as SLAC1 [7-9] and depolarisation-activated channels such as GORK [10,11] with
31 the net result that cations and anions exit guard cells. However, this critically depends on
32 K⁺ release from the vacuole; With ~160 and 100 mM K⁺ in cytoplasm and vacuole of open
33 guard cells [12], vacuolar K⁺ efflux is driven by the negative tonoplast potential and this
34 expels K⁺ from the vacuole via tonoplast K⁺ channels like TPK1. In all, guard cell salt
35 release leads to a loss of turgor that brings about stomatal closure. First we show that the
36 TPK1 vacuolar K⁺ channel is important for ABA and CO₂-mediated stomatal closure. Next
37 we reveal that during ABA and CO₂-mediated closure, TPK1 is phosphorylated and
38 activated by the KIN7 receptor like protein kinase (RLK) which co-expresses in the
39 tonoplast and plasma membrane. The net result is K⁺ release from the vacuole. Taken
40 together our work reveals new components involved in guard cell signalling and describes
41 a new mechanism potentially involved in fine-tuning ABA and CO₂-induced stomatal
42 closure.

43

44 **Results and Discussion**

45 The tonoplast located channel AtTPK1 [13,14] was previously shown to affect ABA-
46 induced stomatal closure in *Arabidopsis* [15]. In this investigation we used patch-clamp

47 electrophysiology to show that GC vacuolar preparations exhibited TPK1 activity (Fig. 1A).
48 Tonoplast channels may show tissue specific properties as was shown for TPC1 [16].
49 However, single channel conductance and weak voltage dependence of GC TPK1 activity
50 were the same as previously reported for TPK1 currents from mesophyll cell vacuoles [15].
51 Addition of 0.5 mM Mg-ATP to the cytoplasmic side of the membrane led to a rapid but
52 moderate increase in channel activity. Channel activity was further increased when both
53 Mg-ATP and 14-3-3 protein were present as was shown previously for TPK1 in mesophyll
54 cells [17,18]. On average, ATP alone caused an increase in channel activity that was
55 equivalent to an increase in open time (and therefore current) of ~50% whereas ATP+14-
56 3-3 more than tripled open probability and current (Figure 1B).

57
58 The S42 residue forms part of the 14-3-3 binding domain in the TPK1 N-terminus and by
59 using a reconstituted TPK1 N-terminus, Latz, et al. [18] showed that S42 phosphorylation
60 is required for TPK1-14-3-3 interaction. To test if the same residue is responsible for the
61 phosphorylation-dependent changes in GC TPK1 activity, we transiently expressed a
62 mutated (S42A) version of TPK1 in the *tpk1* T-DNA knock out background [15]. The S42A
63 version mimics a constitutively non-phosphorylated form. Normal currents were recorded
64 showing that the channel is fully functional (Figure 1A) but the stimulating effects of both
65 ATP and ATP+14-3-3 were abolished (Figure 1B). Taken together these data show that
66 in GCs TPK1 shows low basal activity, which increases after phosphorylation at S42 and
67 is further elevated after binding of 14-3-3. Figure S1 shows that these characteristics were
68 retained when measuring macroscopic currents.

69

70 *ABA causes phosphorylation of TPK1 in planta*

71 Knowing that ABA induces stomatal closure we decided to test whether TPK1
72 phosphorylation is ABA-dependent. GC protoplasts were isolated from the *tpk1* mutant
73 that had been transiently transformed with TPK1::YFP (MW 67.7 kD) and were then
74 probed with a phosphoserine specific antibody that recognised the phosphorylated 14-3-
75 3 binding domain [19]. Figure 1C shows a band around 70 kD that increased in intensity
76 after ABA treatment and was absent in the (non-transformed) *tpk1* null mutant. We also
77 tested if ABA increased TPK1 phosphorylation in intact tissue; treating leaves with 40 μ M
78 ABA for one hour led to increased TPK1 phosphorylation detected in isolated GC
79 protoplasts (Figure 1D). On the basis of densitometry, 2.5-3-fold higher phosphorylation
80 signals were recorded after ABA treatment (Figure 1E). These data allow us to conclude
81 that phosphorylation of TPK1 is regulated by ABA and opens up the possibility that this is
82 part of the GC ABA signalling network and may be necessary for stomatal closure. It would
83 be interesting to further test this idea using a phosphomimic TPK1 version, for example
84 through substitution of S42 with glutamate. Such genotypes could be evaluated for their
85 transpirational flux, steady state stomatal conductance and responses to various stimuli.

86 *A receptor like kinase is involved in TPK1 phosphorylation*

87 To help identify the protein kinase that was responsible for TPK1 phosphorylation we
88 interrogated the SUBA database (<http://suba3.plantenergy.uwa.edu.au/>) for protein
89 kinases that are annotated as tonoplast-localised. A total of 22 kinase isoforms was found
90 and loss of function mutants were obtained for 16 of these (Table S1). Mutants were tested
91 for an altered channel 'activation response' to ATP and 14-3-3 (Figures S2A and S2B and
92 Data S1). The amount of activation generated by ATP varied but was not significantly
93 different between any of the genotypes (Figure S2B). However, activation by ATP+14-3-3
94 was significantly ($p < 0.001$) lower in the *kin7* mutant compared to that observed in WT.

95 Furthermore, a role for KIN7 in TPK1 phosphorylation was confirmed by the large
96 reduction in ABA-induced TPK1 phosphorylation in the *kin7* loss of function mutants
97 (Figure 1E).

98 KIN7 is ubiquitously expressed in all leaf tissues but to investigate whether KIN7 and TPK1
99 physically interact at the GC tonoplast we employed a BiFC strategy [20,21]. Figure 2A
100 shows an intact and an osmotically ruptured GC protoplast co-transformed with TPK1-
101 YFP_{Nt} and TPK1-YFP_{Ct}. As expected, fluorescence is clearly localised in the tonoplast.
102 Similar to the results with TPK1 only, when TPK1-YFP_{Ct} was co-transformed with KIN7-
103 YFP_{Nt} there was a prominent fluorescence signal (Figure 2B, bottom left) in many
104 protoplasts. After osmotic lysis, clear but low intensity fluorescence signal could be
105 observed in the tonoplast of some cells (Figure 2B, bottom right). In contrast, when TPK1-
106 YFP_{Ct} was co-transformed with KIN8-YFP_{Nt} (a kinase very similar to KIN7, see Table S1)
107 no signal was observed in intact or lysed protoplasts (Figure 2C, n>200). BiFC
108 experimentation with KIN12, another comparable kinase (Table S1), produced
109 fluorescence signal but never in the tonoplast (Figure S2, n>200). These results suggest
110 that TPK1 and KIN7 can directly interact at the tonoplast but that either the incidence is
111 low (see Figure S2), or alternatively, that relatively few proteins are involved.

112 Apart from electrophysiology and BiFC, we employed a third strategy to probe TPK1-KIN7
113 interaction. Pull down assays were carried out where the TPK1 N- terminus containing the
114 14-3-3 domain was used as bait [19] and plant extract derived from shoot tissue
115 expressing KIN7::YFP as prey. Figure S3 shows that, in addition to the BiFC and the
116 electrophysiological data, pull down assays too confirm the interaction between TPK1 and
117 KIN7.

118

119 *kin7 and tpk1 are compromised in ABA and CO₂-induced stomatal closure*

120 Previously, we showed that in *tpk1* loss of function mutants ABA-induced stomatal closure
121 is slower than wild type [15]. In the light of our data that TPK1-mediated K⁺ release is likely
122 to depend on KIN7-mediated TPK1 phosphorylation we compared the kinetics of stomatal
123 closure in wild type, *tpk1* and *kin* loss of function mutants. When ABA-induced stomatal
124 closure was measured in *tpk1* a reduced closing response was observed (Figure 2D) as
125 was previously observed [15]. In two independent mutant alleles of *kin7* delayed ABA-
126 induced closure was also observed. When the *kin7-1* line was rescued with a
127 35S:*KIN7:YFP* construct, the transformed line reverted to the wildtype phenotype. These
128 results suggest that TPK1 and KIN7 are part of the GC ABA signalling network. This idea
129 is supported by the observation that ABA dependent TPK1 phosphorylation was greatly
130 reduced in both *kin7* mutants (Figure 1E). To investigate whether TPK1 and KIN7 are
131 involved in other stimuli that cause stomatal closure we exposed the WT, *tpk1* and *kin7*
132 mutants to elevated levels of CO₂. Figure 2E shows that *tpk1* and *kin7* mutants are
133 markedly unresponsive to 1000 ppm CO₂ whether assayed after 3 hours (Figure 2E) or
134 during continuous conductance measurements (Figure S3). These data suggest that
135 TPK1 and KIN7 are also involved in the GC CO₂ signalling network.

136 The latter begs the question whether the KIN7-14-3-3-TPK1 pathway also pertains to other
137 closing stimuli such as the transition from light to dark or a reduction in relative humidity.
138 Preliminary experiments did not show any drought related phenotype in *tpk1* mutants but,
139 since the *tpk1* stomatal phenotype primarily affects closing dynamics rather than the
140 absolute conductance levels [15], more subtle treatments such as alternating relative
141 humidity may be required. Transition to darkness is another stimulus which so far has not
142 been investigated in either the *tpk1* or *kin7* genetic background. Future testing of these

143 and other closing stimuli should help determine whether the signalling mechanism we
144 describe has more general validity.

145

146 *The KIN7 kinase shows dual membrane localisation*

147 As there are reports that KIN7 is localized to the plasma membrane (SUBA:
148 suba2.plantenergy.uwa.edu.au/) we decided to test whether this protein had a dual
149 membrane localization in GCs. To test this we used KIN7::YFP fusion proteins which were
150 stably expressed under control of the 35S promoter or the endogenous KIN7 promoter. In
151 GC protoplasts derived from transgenic lines, KIN7-YFP was occasionally observed in
152 both plasma membrane and tonoplast (Figure 3A-F). However, in most cases plasma
153 membrane signal greatly predominated (Figure 3C and D) to the extent that the tonoplast
154 signal was only detected after osmotic lysis (Figure 3E and F) when weak but distinct
155 fluorescence can be distinguished in a proportion of cells as was seen in the BiFC
156 experiments. This pattern was consistent for KIN7-YFP expression, irrespective of the
157 promoter driving expression (Figure S4) and clearly point to dual localisation of KIN7. The
158 latter prompted us to investigate whether KIN7 localisation is sensitive to ABA. One half
159 of a KIN7-YFP transformed GC population was treated with 40 μ M ABA and subsequently
160 the proportion of protoplasts with tonoplast located signal was determined. Figure 3G
161 shows that the fraction of cells with tonoplast signal more than doubles after exposure to
162 ABA in a time dependent manner. To independently confirm these findings, we carried out
163 Western analyses on tonoplast enriched membrane fractions using the tonoplast
164 aquaporin TIP1;1 as a tonoplast specific marker [22]. Figure 3H shows that initially there
165 is a minimal KIN7 signal in the lower phase of a two phase partitioned membrane prep.
166 However, relative to the tonoplast marker TIP1;1, and within 30 min ABA exposure, the

167 KIN7 signal is greatly enhanced, to more than 4-fold the initial value (Figure 3I) while
168 similar experiments using high CO₂ treatment (1000 ppm, 3h) showed comparable results
169 with an approximately 3-fold increase towards tonoplast expression (Figure S4). These
170 results show that ABA may affect TPK1 activity in less than 30 minutes. Cation flux
171 measurements from *Commelina* epidermal strips [23] show remarkably similar kinetics of
172 10-20 minutes between ABA addition and cation release. However, these values are
173 considerably slower than what has been seen for some plasma membrane anion
174 channels. For example, Levshenko et al [24] recorded anion channel activation 1-2
175 minutes after ABA exposure. There may be several explanations for this difference; Anion
176 channel activation is one of the first responses to ABA and may therefore precede slower
177 cation channel activation. TPK1 activation in intact tissue may be accelerated by unknown
178 cell wall components or, alternatively, different ABA receptors may be involved in the
179 coupling to various membranes.

180 The above results show that ABA and CO₂ treatment led to an increase in tonoplast KIN7
181 signal. The data do not allow to distinguish whether elevated tonoplast expression was
182 due to *de novo* expression or a consequence of intracellular trafficking. However,
183 preliminary experiments where tissue was treated with cycloheximide (a protein synthesis
184 inhibitor) or chlorpromazine (an endocytosis inhibitor) suggest that tonoplast KIN7
185 expression was not affected by cycloheximide (Figure S4) but sensitive to chlorpromazine.
186 Such results suggest that endocytosis, rather than *de novo* protein synthesis, is an
187 essential feature of the shift in KIN7 expression toward the tonoplast.

188 *Conclusions*

189 There is a number of conclusions that can be drawn from our work. Our data showing that
190 TPK1 and KIN7 are involved in CO₂ and ABA is further evidence that both these closure

191 signals are able to access a common set of signalling components whose role it is to bring
192 about stomatal closure [25]. In addition to identifying that TPK1 activity is regulated by
193 protein phosphorylation we also report the identity of the regulatory protein kinase. KIN7
194 has all the hallmarks of an LRR-receptor kinase. It is ubiquitously expressed in many
195 tissues, including mesophyll cells. In addition to GCs, mesophyll cells have been shown
196 to respond to ABA, for example by reducing cell volume (e.g. [26]). This opens the
197 possibility that in mesophyll cells too, KIN7-mediated TPK1 activation plays a role in ABA
198 signalling. Preliminary patch clamp recordings suggest that KIN7 does impact on TPK1
199 activity in mesophyll cells which supports the above idea but whether this is linked to
200 phosphorylation and 14-3-3 binding of mesophyll cell TPK1 remains to be tested.

201 Another major questions to emerge from our work is, what is the link between perception
202 of ABA and CO₂ on the one hand, and activation of KIN7, binding of 14-3-3 and activation
203 of TPK1 on the other? Upstream signalling components could include well known players
204 such as ABI and OST gene products. Further experimentation with ABA signalling
205 mutants, or ones in CO₂ signalling components such as HT1 kinase, RHC1 and RBOH-
206 D/F, will help reveal such interactors. Downstream, 14-3-3 must bring about a
207 conformational change that greatly stimulates channel opening. One mechanism suggests
208 that the TPK1 gate is directly controlled via Ca²⁺ binding to C-terminal EF domains [27]
209 and a model where 14-3-3 sensitises TPK1 Ca²⁺ dependence not only provides a
210 mechanistic explanation but could be tested using electrophysiology.

211 It is noteworthy that ABA treatment has been reported to result in KIN7 phosphorylation at
212 its C-terminus [28]. If the phosphorylation results in alterations to KIN7 activity this would
213 suggest that at least one additional protein kinase is involved in this signalling network.

214 Our data showing that KIN7 is localized at both the plasma and tonoplast membranes is

215 supportive of a dynamic, stimulus-induced, mechanism of TPK1 regulation. Inhibition by
216 the endocytotic inhibitor chlorpromazine of the relative shift toward tonoplast expression
217 of KIN7 suggests that the observed increase in KIN7 tonoplast localisation does not
218 originate from de novo KIN7 biosynthesis, but occurs via a hitherto uncharacterised
219 trafficking pathway. Although such findings can only be preliminary and will need further
220 support, retrograde endocytotic trafficking of plasma membrane proteins to
221 endocompartments has been reported: In animals compartmentalisation of receptor
222 kinases generates endosome specific signal transduction complexes [29]. In plants too,
223 trafficking of the steroid receptor kinase BRI1 to endosomal vesicles is believed to be
224 important in intracellular signalling [30].

225 Control of TPK1 activity through the stimulus-induced localization of KIN7, be it via
226 modulation of expression or via trafficking, represents an attractive mechanism for exerting
227 control over K^+ efflux from vacuoles. We have summarised what we know about this
228 pathway in the schema described in Figure 4. What might be the function of this form of
229 regulation? Our phenotypic data showing that mutants in this pathway are distinguished
230 by exhibiting slower rates of closure suggest that this pathway might be in the fine-tuning
231 of stomatal responses rather than switching closure on (or off). However, a better
232 understanding awaits the discovery of additional components in the network.

233 **ACKNOWLEDGEMENTS:** We thank Bert de Boer (Vrije Universiteit Amsterdam) for his
234 kind gift of 14-3-3 protein and Ingo Dreyer (Universidad de Talca, Chile) for his kind gift of
235 BiFC vectors. We thank Wioletta Pijacka (University of Bristol, UK) for her technical help
236 with Western blotting. AMH and J-C I wish to acknowledge grant support from the UK
237 BBSRC (BB/J002364/1) and the Leverhulme Trust.

238 **AUTHOR CONTRIBUTIONS:**

239 JCI and FJM designed research; JCI, FJM, AB and TSN performed research; JCI and
240 FJM analysed data; FJM, AMH and JCI wrote the paper.

241 **DECLARATION OF INTERESTS**

242 The authors declare no competing interests.

243 **REFERENCES**

- 244 1. Hetherington, A.M., and Woodward, F.I. (2003). The role of stomata in sensing and driving
245 environmental change. *Nature*. *424*, 901-908.
- 246 2. Roelfsema, M.R., Levchenko, V., and Hedrich, R. (2004). ABA depolarizes guard cells in
247 intact plants, through a transient activation of R- and S-type anion channels. *Plant J.* *37*, 578-588.
- 248 3. Schroeder, J., Gethyn J Allen, Veronique Hugouvieux, June M Kwak, a., and Waner, D.
249 (2001). Guard cell signal transduction. *Annu Rev Plant Physiol Plant Mol Biol.* *52*, 627-658.
- 250 4. Assmann, S.M., and Jegla, T. (2016) Guard cell sensory systems: recent insights on stomatal
251 responses to light, ABA and CO₂. *Curr Opinion Plant Biology* *33*, 157-167.
- 252 5. Raghavendra, A.S., Gonugunta, V.K., Christmann, A., and Grill, E. (2010) ABA perception
253 and signalling. *Trends in Plant Sciences* *15*, 395-401.
- 254 6. Munemasa, S., Hauser, F., Park, J., Waadt, R., Brandt, B., and Schroeder, J.I. (2015)
255 Mechanisms of ABA-mediated control of stomatal aperture. *Current Opinion in Plant Biology* *28*,
256 154-162.
- 257 7. Geiger, D., Maierhofer, T., AL-Rasheid, K.A.S., Scherzer, S., Mumm, P., Liese, A., Ache,
258 P., Wellmann, C., Marten, I., Grill, E., et al. (2011). Stomatal closure by fast abscisic acid signaling
259 is mediated by the guard cell anion channel SLAH3 and the receptor RCAR1. *Sci Signal.* *4*, ra32.
- 260 8. Geiger, D., Scherzer, S., Mumm, P., Stange, A., Marten, I., Bauer, H., Ache, P., Matschi,
261 S., Liese, A., Al-Rasheid, K.A.S., et al. (2009). Activity of guard cell anion channel SLAC1 is
262 controlled by drought-stress signaling kinase-phosphatase pair. *Proc Natl Acad Sci USA.* *106*,
263 21425-21430.
- 264 9. Imes, D., Mumm, P., Bohm, J., Al-Rasheid, K.A., Marten, I., Geiger, D., and Hedrich, R.
265 (2013). Open stomata 1 (OST1) kinase controls R-type anion channel QUAC1 in *Arabidopsis* guard
266 cells. *Plant J.* *74*, 372-382.
- 267 10. Ache, P., Becker, D., Ivashikina, N., Dietrich, P., Roelfsema, M.R., Hedrich, R. (2000).
268 GORK, a delayed outward rectifier expressed in guard cells of *Arabidopsis thaliana*, is a K(+)-
269 selective, K(+)-sensing ion channel. *FEBS Lett.* *486*, 93-98.
- 270 11. Hosy, E., Vavasseur, A., Mouline, K., Dreyer, I., Gaymard, F., Porée, F., Boucherez, J.,
271 Lebaudy, A., Bouchez, D., Véry, A.-A., et al. (2003). The *Arabidopsis* outward K⁺ channel GORK
272 is involved in regulation of stomatal movements and plant transpiration. *Proc Natl Acad Sci USA.*
273 *100*, 5549-5554.
- 274 12. Hills, A., Chen, Z.H., Amtmann, A., Blatt, M.R., Lew, V.L. (2012). OnGuard, a
275 Computational Platform for Quantitative Kinetic Modeling of Guard Cell Physiology. *Plant*
276 *Physiol.* *159*(3):1026-42.
- 277 13. Dunkel, M., Latz, A., Schumacher, K., Muller, T., Becker, D., and Hedrich, R. (2008).
278 Targeting of vacuolar membrane localized members of the TPK channel family. *Mol Plant.* *1*, 938-
279 949.

- 280 14. Voelker, C., Gomez-Porrás, J.L., Becker, D., Hamamoto, S., Uozumi, N., Gambale, F.,
 281 Mueller-Roeber, B., Czempinski, K., and Dreyer, I. (2010). Roles of tandem-pore K⁺ channels in
 282 plants - a puzzle still to be solved. *Plant Biol* 12 *Suppl* 1, 56-63.
- 283 15. Gobert, A., Isayenkov, S., Voelker, C., Czempinski, K., and Maathuis, F.J. (2007). The two-
 284 pore channel TPK1 gene encodes the vacuolar K⁺ conductance and plays a role in K⁺ homeostasis.
 285 *Proc Natl Acad Sci USA*. 104, 10726-10731.
- 286 16. Rienmüller, F., Beyhl, D., Lautner, S., Fromm, J., Al-Rasheid, K.A., Ache, P., Farmer, E.E.,
 287 Marten, I., Hedrich, R. (2010) Guard cell-specific calcium sensitivity of high density and activity
 288 SV/TPC1 channels. *Plant Cell Physiol*. 51, 1548-54.
- 289 17. Isayenkov, S., Isner, J.C., and Maathuis, F.J. (2011). Rice two-pore K⁺ channels are
 290 expressed in different types of vacuoles. *Plant Cell*. 23, 756-768.
- 291 18. Latz, A., Becker, D., Hekman, M., Müller, T., Beyhl, D., Marten, I., Eing, C., Fischer, A.,
 292 Dunkel, M., Bertl, A., et al. (2007). TPK1, a Ca²⁺-regulated *Arabidopsis* vacuole two-pore K⁺
 293 channel is activated by 14-3-3 proteins. *Plant J*. 52, 449-459.
- 294 19. Latz, A., Mehlmer, N., Zapf, S., Mueller, T.D., Wurzinger, B., Pfister, B., Csaszar, E.,
 295 Hedrich, R., Teige, M., and Becker, D. (2013). Salt stress triggers phosphorylation of the
 296 *Arabidopsis* vacuolar K⁺ channel TPK1 by calcium-dependent protein kinases (CDPKs). *Mol Plant*.
 297 6, 1274-1289.
- 298 20. Waadt, R., Schmidt, L.K., Lohse, M., Hashimoto, K., Bock, R., and Kudla, J. (2008).
 299 Multicolor bimolecular fluorescence complementation reveals simultaneous formation of
 300 alternative CBL/CIPK complexes in planta. *Plant J*. 56, 505-516.
- 301 21. Kudla, J., and Bock, R. (2016). Lighting the way to protein-protein interactions:
 302 Recommendations on best practices for bimolecular fluorescence complementation analyses. *Plant*
 303 *Cell*. 28, 1002-1008.
- 304 22. Ludevid, D., Hofte, H., Himmelblau, E., and Chrispeels, M.J. (1992). The expression pattern
 305 of the tonoplast intrinsic protein gamma-tip in *Arabidopsis thaliana* is correlated with cell
 306 enlargement. *Plant Physiol*. 100, 1633-1639.
- 307 23. MacRobbie EA (2006) Control of volume and turgor in stomatal guard cells. *J Membr Biol*
 308 210: 131-42
- 309 24. Levchenko, V., Konrad, K.R., Dietrich, P., Roelfsema, M.R., Hedrich, R.(2005). Cytosolic
 310 abscisic acid activates guard cell anion channels without preceding Ca²⁺ signals. *Proc Natl Acad*
 311 *Sci U S A*. 15;102(11):4203-8.
- 312 25. Chater, C., Peng, K., Movahedi, M., Dunn, Jessica A., Walker, Heather J., Liang, Y.-K.,
 313 McLachlan, Deirdre H., Casson, S., Isner, Jean C., Wilson, I., et al. Elevated CO₂-induced
 314 responses in stomata require ABA and ABA signaling. *Curr Biol*. 25, 2709-2716.
- 315 26. Kolla, V.A., Suhita, D., Raghavendra, A.S. (2004) Marked changes in volume of mesophyll
 316 protoplasts of pea (*Pisum sativum*) on exposure to growth hormones. *J Plant Physiol*. 161, 557-562.
- 317 27. Hartley, T.N., Maathuis, F.J.M. (2015) Allelic variation in the vacuolar TPK1 channel
 318 affects its calcium dependence. *FEBS Lett*. 590, 110-117.
- 319 28. Chen, Y., Hoehenwarter, W., and Weckwerth, W. (2010). Comparative analysis of
 320 phytohormone-responsive phosphoproteins in *Arabidopsis thaliana* using TiO₂-phosphopeptide
 321 enrichment and mass accuracy precursor alignment. *Plant J*. 63, 1-17.
- 322 29. Villaseñor, R., Nonaka, H., Del Conte-Zerial, P., Kalaidzidis, Y., and Zerial, M. (2015).
 323 Regulation of EGFR signal transduction by analogue-to-digital conversion in endosomes. *eLife*. 4,
 324 e06156.
- 325 30. Geldner, N., and Robatzek, S. (2008). Plant receptors go endosomal: a moving view on
 326 signal transduction. *Plant Physiol*. 147, 1565-1574.

- 327 31. Schindelin, J., Rueden, C.T., Hiner, M.C., and Eliceiri, K.W. (2015). The ImageJ
328 ecosystem: An open platform for biomedical image analysis. *Mol Reprod Dev.* 82, 518-529.
- 329 32. Pijacka, W., Clifford, B., Tilburgs, C., Joles, J.A., Langley-Evans, S., and McMullen, S.
330 (2015). Protective role of female gender in programmed accelerated renal aging in the rat. *Physiol*
331 *Rep.* 3.
- 332 33. Hellens, R., Edwards, E.A., Leyland, N., Bean, S., and Mullineaux, P. (2000). pGreen: a
333 versatile and flexible binary Ti vector for *Agrobacterium*-mediated plant transformation. *Plant Mol*
334 *Biol.* 42, 819-832.
- 335 34. Pandey, S., Wang, X.Q., Coursol, S.A., and Assmann, S.M. (2002). Preparation and
336 applications of *Arabidopsis thaliana* guard cell protoplasts. *New Phytol.* 153, 517-526.
- 337 35. Maathuis, F.J.M., May, S.T., Graham, N.S., Bowen, H.C., Jelitto, T.C., Trimmer, P.,
338 Bennett, M.J., Sanders, D., and White, P.J. (1998). Cell marking in *Arabidopsis thaliana* and its
339 application to patch-clamp studies. *Plant J.* 15, 843-851.
- 340 36. Sinnige, M.P., Roobeek, I., Bunney, T.D., Visser, A.J., Mol, J.N., and de Boer, A.H. (2005).
341 Single amino acid variation in barley 14-3-3 proteins leads to functional isoform specificity in the
342 regulation of nitrate reductase. *Plant J.* 44, 1001-1009.
- 343 37. Lund, A., and Fuglsang, A.T. (2012). Purification of plant plasma membranes by two-phase
344 partitioning and measurement of H⁺ pumping. *Methods Mol Biol.* 913, 217-223.
- 345 38. Rea, P.A., Britten, C.J., and Sarafian, V. (1992). Common identity of substrate binding
346 subunit of vacuolar H⁺-translocating inorganic pyrophosphatase of higher plant cells. *Plant Physiol.*
347 *100*, 723-732.
- 348

349 **Figure legends:**

350 **Figure 1: GC TPK1 currents and ABA induced TPK1 phosphorylation.**

351 **(A)** Representative TPK1 currents from one cytoplasmic side out excised patch shows
352 TPK1 currents in control buffer, after addition of MgATP (0.5 mM) or MgATP plus 14-3-
353 3 (100 nM). Mutation of the N-terminal serine 42 to alanine (S42A) leaves channel
354 activity intact but abrogates the effect of ATP and 14-3-3. Currents were recorded at -
355 40 mV and left side arrows indicate closed levels. Amplitude histograms on right show
356 increase in channel openings for wildtype but not S42A. 'Po' open probability
357 quantification based on 60 sec records. **(B)** Normalised relative channel activity, based
358 on open probability data obtained at -80 mV, showing ATP stimulates activity by around
359 45% and ATP plus 14-3-3 stimulates activity by over 300%, while no significant effect of
360 ATP+14-3-3 is observed for the S42A mutant protein (n=3 independent membrane

361 patches for each condition, error bars are standard errors.) Data were analysed using
362 one way ANOVA with Tukey post-hoc analysis comparison with control conditions,
363 asterisks denoting $p < 0.05$. **(C)** GCs from *tpk1* plants were isolated and transiently
364 transformed with TPK1-YFP. Approx 12-16h after transformation half the protoplasts
365 were treated with ABA (1h, 40 μ M). Right hand panel: non transformed (NT) protoplasts
366 show complete absence of signal ('T' are transformed protoplasts from the same prep).
367 **(D)** Guard cells isolated from ABA-treated *tpk1* loss of function plants, control leaves
368 (WT plants) or ABA treated leaves (WT plants). In (C) and (D), top panels show typical
369 example of blots with antibody against the phosphorylated TPK1 N-terminus. Bottom
370 panels show total protein staining. **(E)** Densitometry based (n=3, bars denote standard
371 errors) fold-changes in TPK1 phosphorylation in control (WT-con) and ABA treated
372 (WT_ABA_L) leaves or protoplasts (WT_ABA_P) and in null mutants of the LRR kinase
373 KIN7 (*kin7_ABA*). Data were analysed using one way ANOVA with Tukey post-hoc
374 analysis comparison with control conditions, asterisks denoting $p < 0.05$. (See also
375 Figures S1 and Table S1).

376 **Figure 2: Bimolecular fluorescence complementation and loss of function**
377 **phenotypes in *tpk1* and *kin7*.**

378 **(A)** Representative image for Arabidopsis GCs cotransformed with TPK1_{YFP-Nt} plus
379 TPK1_{YFP-Ct}. Note clear vacuolar fluorescence. **(B)** GC protoplasts expressing KIN7_{YFP-}
380 _{Nt} plus TPK1_{YFP-Ct}. Note clear signal in the tonoplast. **(C)** GC protoplast expressing
381 KIN8_{YFP-Nt} plus TPK1_{YFP-Ct}. Note the absence of any fluorescence signal. In all cases,
382 top two panels show DIG images of intact and osmotically ruptured protoplast (releasing
383 the large central vacuole). Bottom panels show corresponding YFP fluorescence signal.
384 Scale bar is 5 μ m. **(D)** Leaves of wild type (WT), TPK1 and KIN7 loss of function mutants

385 KIN7 complemented plants were exposed to 100, 10 or 1 μ M ABA and start ('Control')
386 and end (30 minute ABA exposure) conductance values were recorded. **(E)** Stomata
387 were opened by exposure of leaves to 400 ppm CO₂ for 2 hours. Subsequently, peels
388 were either aerated with 1000 ppm [CO₂] or continued to be aerated with 400 ppm [CO₂].
389 Three hours later, stomatal apertures were measured. Data in D and E were analysed
390 for significance using a one way ANOVA with Tukey post-hoc analysis. Asterisk denotes
391 $p < 0.05$. (See also Figures S2 and S3).

392 **Figure 3: KIN7:YFP expression patterns.**

393 **(A)** DIC image of intact Arabidopsis GC transformed with KIN7:YFP. **(B)** Corresponding
394 fluorescence image showing expression in both plasma membrane and tonoplast
395 (arrows). **(C and D)** DIC and fluorescence image of GC protoplast showing prominent
396 expression in the plasma membrane only. **(E)** DIC image of osmotically ruptured
397 protoplast releasing the large vacuole. **(F)** Corresponding fluorescence image showing
398 weak but distinct tonoplast expression. **(G)** The proportion of lysed guard cell
399 protoplasts that shows tonoplast KIN7 expression increases after ABA treatment. **(H)**
400 Western immunoblot showing increasing level of KIN7-GFP expression in response to
401 ABA. The vacuole specific aquaporin TIP1;1 was used as tonoplast marker whereas the
402 lack of cross reactivity with the H⁺-ATPase AHA1 (a plasma membrane specific marker)
403 in the 'lower phase' (LP) shows absence of plasma membrane. 'MF': microsomal
404 fraction showing positive reactivity for all three probes. **(I)** Quantification based on
405 densitometry measurements (using ImageJ) of relative increase in KIN7 expression in
406 the tonoplast. Scale bar in A-F is 7 μ m. Data depicted in G and I are based on 3 or more
407 independent experiments, bars denote standard errors and data were analysed using

408 one way ANOVA with Tukey post-hoc analysis comparison with control conditions.

409 Asterisk denotes $p < 0.05$. (See also Figure S4).

410 **Figure 4: A model for coupling ABA and TPK1.**

411 ABA perception leads to activation of the LRR kinase KIN7. Increased tonoplast

412 expression of KIN7 and/or KIN7 traffic from plasma membrane (PM) to tonoplast (TO)

413 brings KIN7 in the vicinity of TPK1. At the tonoplast, phosphorylation of S42 in the N-

414 terminal 14-3-3 binding domain allows 14-3-3 binding to TPK1, which leads to drastically

415 increased TPK1 activity and stomatal closure.

416 **METHODS**

417 **CONTACT FOR REAGENT AND RESOURCE SHARING**

418 Further information and requests for resources and reagents should be directed to and

419 will be fulfilled by the Lead Contact, Frans Maathuis (frans.maathuis@york.ac.uk)

420 **EXPERIMENTAL MODEL AND SUBJECT DETAILS**

421 **Plant material and growth.** *Arabidopsis thaliana* (L) ecotype Columbia (0) wild type,

422 *tpk1* (SALK line 146903; [15] and kinase mutants and kinase mutants obtained from

423 NASC (see Table S1).

424 **METHOD DETAILS**

425 **Plants**

426 *Arabidopsis thaliana* (L) ecotype Columbia (0) wild type, *tpk1* and kinase mutants were grown for

427 3 to 4 weeks in soil (F2, Levington, UK) at 18/22°C night/day temperature in a glasshouse with day

428 lengths of 14 h, supplemented with artificial light of around $200 \mu\text{mol m}^{-2} \text{sec}^{-1}$ as described [17].

429 T-DNA insertion lines for kinase mutants and the forward and reverse primers that were used to test

430 for homozygosity and transcript can be found in Table S1 and S2.

431 **Cloning of kinases in the BiFC vector**

432 KIN8 and KIN12 were cloned from cDNA produced from total RNA: Total RNA was extracted

433 from *Arabidopsis* leaves with RNeasy Plant Mini Kit (Qiagen GmbH, Germany). First strand cDNA

434 was synthesised using SuperScript II Reverse Transcriptase kit (Life Technologies Ltd, UK) with
435 the following primers: kin8bifc fwd and kin8bifc rev, kin12bifc fwd and kin12bifc rev (Table S2).
436 KIN8 and KIN12 fragments were amplified using kin8bifc fwd+kin8bifc rev and kin12bifc fwd+
437 kin12bifc rev primers respectively (Table S2). KIN7 was PCR-amplified from the full length cDNA
438 clone U12357 (<http://abrc.osu.edu/>) using the kin7bifc fwd and kin7bifc rev primers (Table S2).
439 Amplified fragments were digested using SpeI and XhoI for KIN7 and KIN8 or BamHI and XhoI
440 for KIN12 and inserted in pSPYNE [20].

441 **Quantification of BiFC signals**

442 To be able to compare BiFC signals from various combinations, ImageJ software [31]) was used to
443 measure signal intensity from the vacuolar and plasma membranes. Values were corrected by
444 subtracting signal intensity from nearby background. Signal from TPK1_YFP_Nt+TPK1_YFP_Ct
445 (which forms a dimer) was used as positive control and the signal from
446 kin12_YFP_Nt+TPK1_YFP_Ct (which shows signal in ER and PM but not, or extremely little, in
447 the tonoplast) used as negative control. Quantitative data for BiFC fluorescence signal are shown in
448 Figure S2.

449 **TPK1 pull-down assay**

450 Pull-down assays were used to confirm the interaction between the N-terminus part of TPK1 and
451 KIN7. The sequence corresponding to the first 81 amino acids of TPK1 (NTPK1) was amplified by
452 PCR using tpk1bamhI and tpk1xhoI primers (Table S2) and cloned into the pGEX6P-1 vector
453 (GE Healthcare, Amersham, UK). GST and GST::NTPK1 expression was induced in 1l culture of
454 *E. coli* BL21 at 37°C with 1mM IPTG for 4 hours. Cells were collected and lysed in PBS-T buffer
455 (PBS pH 7.3, 0.1% Trion X-100) by sonication. After centrifugation, the lysate was cleared using
456 0.45 µm filters. GST or GST::NTPK1 was bound to 500 µl of Glutathione Sepharose 4B (GE
457 Healthcare, Amersham, UK) for 2h. 50 µl bead aliquots washed with buffer P (HEPES 50mM
458 pH7.3, 2mM CaCl₂, 2mM MgCl₂, 2mM KCl, 100mM NaCl, 1% CHAPS) and protease inhibitor
459 cocktail IV (Calbiochem, Merck, Feltham, UK) were incubated overnight with either proteins
460 extracted with buffer P from plants expressing wild type KIN7 or KIN7::YFP. The next day, beads
461 were washed 4 times with the same buffer. Bound proteins were eluted with SDS-PAGE Protein
462 Sample Buffer (2×) and loaded on a 10% acrylamide gel. Western blotting was performed as
463 described previously [32]. Rabbit anti-GFP (ThermoFisher, Paisley, UK) and swine anti-rabbit
464 Immunoglobulins HRP (Agilent, Stockport, UK) were used and the resulting signal in the presence

465 of Luminata Forte substrate (Merck, Feltham, UK) was imaged with Fusion Pulse imaging system
466 (Vilber Lourmat, Marne-la-Vallée, France).

467 **Cloning of KIN7:YFP and Arabidopsis plant transformation**

468 KIN7 was PCR amplified from the clone U12357 (<http://abrc.osu.edu/>) with the kin7yfpfwd and
469 kin7yfprev primers (Table S2) and inserted in the pART7 vector [33]. The NotI fragment containing
470 the 35S::KIN7:YFP fragment was subsequently inserted in pGREEN0229. *Arabidopsis* plants were
471 transformed by floral spraying as described in [33]. Briefly, *Agrobacterium* was grown in 50 mL
472 liquid YEB medium for two days or until the OD reached 3. The cells were spun down (5 min,
473 4000g) and resuspended in 20 mL of 0.1x MS medium, 5% sugar, 0.1% Silwet L-77, pH 5.7. Every
474 two weeks, flowering plants were sprayed with *Agrobacterium* using an airbrush. For
475 pKin7::KIN7:YFP, 589bp upstream of the ATG was amplified from genomic DNA with
476 promkin7fwd and promkin7rev primer (Table S2). This Fragment was inserted in the
477 35S::KIN7::YFP vector instead of the 35S promoter, which was removed using StuI and XhoI.

478 **Protoplast isolation:**

479 Guard cell protoplasts were isolated as described by Pandey, et al. [34]. 40 fully expanded leaves
480 were blended in water for 1 minute using a waring SS515 Blender (Cole-Parmer UK) and poured
481 onto a 200 µm mesh to collect epidermes. Epidermes were incubated in 45% H₂O, 55% basic
482 solution (0.5 mM CaCl₂, 0.5mM MgCl₂, 0.01 mM KH₂PO₄, 0.5 mM ascorbic acid, 550 mM
483 sorbitol, 0.2% BSA, 0.7% cellulysin, 5 mM MES/Tris pH 5.5) for 1.5 h at 30°C. The epidermes
484 were then incubated in basic solution supplemented with cellulase Onozuka RS 0.01% and
485 pectolyase Y23 for 1 h at 30°C. Guard cell protoplasts were collected after passing the solution
486 through a 20 µm mesh.

487 Mesophyll protoplast were extracted from Arabidopsis leaves according to [Isayenkov, 2011 #4].
488 Leaves were cut in 1-mm sections and digested for 4 h in an enzyme solution containing 1.5%
489 cellulose RS, 0.75% macerozyme, 0.6 m mannitol, 10 mM 2-(N-morpholine)-ethanesulphonic acid
490 (MES), pH 5.6 and 1 mM CaCl₂, in which proteases were heat inactivated for 10 min at 55°C.
491 Protoplasts were filtered and centrifuged for 3 min at 500 g and resuspended in protoplast incubation
492 solution (0.6 M mannitol, 4 mM MES, pH 5.7, 4 mM KCl and 3 mM CaCl₂)

493 **Electrophysiology**

494 Vacuole release, equipment and analyses were as described in Maathuis, et al. [35]. After transfer
495 of protoplasts to the recording chamber, vacuoles were released by washing protoplasts with a

496 solution containing 10 mM EDTA, 10 mM EGTA, pH 8 with an osmolarity of 350 mOsm. Standard
497 experimental solutions for bath and pipette contained 100 mM KCl, 0.1 mM CaCl₂, 5 mM MES/Tris
498 pH 7 and sorbitol adjusted to 430 mOsm total osmolarity. Open probability (Po) was calculated as
499 described in Gobert, et al. [15] and defined as: $Po = (t_{open}/t_{total})/n$ where 'n' is an estimate of
500 the number of channels in the membrane patch derived from the maximum number of open levels
501 observed in the recording. Recordings of 60 s duration (t_{total}) at a membrane potential of -80 mV
502 were analysed by using a 50% threshold technique to define current transitions and calculate t_{open}
503 to determine Po. Open probability data were obtained from 3 to 10 individual protoplasts (see Figure
504 S2 and Data S1). To compare different genotypes, the increase in Po in response to ATP and
505 ATP+14-3-3 was calculated for each experiment and 'fold changes' were subsequently averaged
506 across experiments. ATP was added as Mg-ATP at a final concentration of 0.5 mM. 14-3-3 protein
507 (as Hv14-3-3B or Hv14-3-3C; GenBank accessions X93170 and Y14200 respectively [36]) was a
508 kind gift from Bert de Boer (Vrije Universiteit, Amsterdam) and added to a final concentration of
509 0.2 µg/ml.

510 **Imaging**

511 Intact and osmotically disrupted guard cells were photographed on a Zeiss epifluorescence
512 microscope using bright light, DIC or epifluorescence (465-495 nm excitation and 515 nm emission
513 wavelength) with a 20x, 40x or 63x objective. Confocal imaging was performed using a Zeiss
514 LSM510 Meta microscope (Carl Zeiss, <http://www.zeiss.com>).

515 **Leaf Stomatal conductance and apertures**

516 To record responses to ABA, leaves of mature plants were removed at approx 10:00h and incubated
517 in 'opening' buffer (10 mM KCl, 10 mM MES-KOH pH 6.15) for 2 h in the light to induce
518 maximum opening. Subsequently, H₂O gas exchange was determined (in the same buffer) using an
519 infrared gas analyser, Li-Cor 6400 (LI-COR, Cambridge, UK) to obtain a starting conductance
520 value. Subsequent values were obtained after 30 min incubation in control (no ABA) or ABA (1,
521 10 or 100 µM final concentration) buffer. Each experiment was carried out using three leaves and
522 in total 12-24 leaves from 3-4 individual plants were used for each treatment. Changes recorded in
523 control treatments (no ABA) were subtracted from those obtained from ABA treated leaves.

524 To obtain time courses for the response to elevated [CO₂], stomatal conductance was measured
525 using infrared gas analysis. Measurements were performed using a portable photosynthesis system
526 attached to a leaf chamber with a 2.5 cm² leaf area (Walz GFS-3000). CO₂ was scrubbed from

527 external air using soda lime and resupplied from a liquid CO₂ cartridge to maintain CO₂
528 concentrations of either 400 or 1000 ppm. Temperature was maintained at 22°C and the absolute
529 humidity to 16000 ppm to obtain a relative humidity of 64.5%. Air flow was 400 μmol.s⁻¹, light
530 intensity was 120 μmol.m⁻².s⁻¹. For each measurement, an individual mature leaf was placed in the
531 leaf chamber, while still attached to the plant. Leaves were left in the chamber for 30 min before
532 measurements were taken to allow them to acclimatise to chamber conditions and for gas exchange
533 to stabilise. Measurements were then logged every 10 secs and averaged every 2.5 min. Data
534 represent the mean +-SEM from 3 different plants.

535 To obtain stomatal apertures, leaf epidermes were removed from fully expanded leaves of 5 to 6
536 week old plants. They were collected cuticle-side up on CO₂-free 10 mM MES/KOH (pH 6.15) in
537 5cm Petri dishes (Sterilin, UK) at 22°C for 30min. Epidermal peels were transferred to fresh Petri
538 dishes and incubated in the light under a fluence rate of 120 μmol.m⁻².s⁻¹ in 50mM KCl, 10 mM
539 MES/KOH (pH 6.15) at 22°C 2 hours whilst being aerated with an air stream containing 400 ppm
540 [CO₂] from a pressurised cylinder (BOC, Special Gasses, UK) by bubbling directly into the buffer.
541 Subsequently, peels were either aerated with 1000ppm [CO₂] or continued to be aerated with
542 400ppm [CO₂]. After 3h, peels were removed, mounted on slides and measurements of stomatal
543 aperture were recorded using an inverted microscope (Leica DM-IRB, Leica UK). Forty stomatal
544 pores were measured per treatment in three separate replicated experiments (total stomatal number
545 = 120; n = 3). To avoid bias, experiments were performed without knowing the identity of the plants
546 and the treatments until data were collected. Data were analysed using one-way ANOVA.

547 **Immunoblotting**

548 Guard cell protoplast preparations were visually inspected and only used when containing fewer
549 than 1% mesophyll protoplasts. ABA treatment (40 μM, 1 hour) was either done on intact leaves in
550 buffer (containing 20 mM KCl, 10 mM MES/KOH pH 6.1) at ~150 μmol.s⁻¹.m⁻² light, or on isolated
551 protoplasts in buffer (containing 500 mM Sorbitol, 10 mM KCl, 1 mM CaCl₂, 10 mM MES/Tris
552 pH 5.5). In the latter case, protoplasts were isolated from *tpk1* mutants, and transiently transformed
553 with pART7:TPK1:YFP [15]. Around 16h after transformation, protoplasts were divided in two
554 population with one exposed to ABA (conditions as above). After treatment, protoplasts were
555 resuspended in 'RIPA' buffer (1% Triton X 100, 0.1% SDS, 100 mM NaCl, 10 mM Na₂HPO₄ and
556 10 mM NaH₂PO₄, pH 7.2 plus protease inhibitor cocktail 'cComplete EDTA free' from Roche UK)
557 and stored at -20°C.

558 For analysis of phosphorylation levels, protein samples (40µg) were precipitated by methanol-
559 chloroform extraction, separated by SDS-10% acrylamide gel electrophoresis and transferred onto
560 nitrocellulose (Hybond-ECL, GE Healthcare). Prior to blocking (5% BSA, TBS), protein levels
561 were visualised with Ponceau S (0.1% w/v in 1% Acetic acid). TPK1 phosphorylation was detected
562 by immunoblotting overnight with anti-pBAD-Ser136 (1:200, i.e. 75 µL in 15 ml, rabbit polyclonal
563 serum, Santa Cruz sc-12969; secondary antibody IRDye 800CW Donkey anti-rabbit, LI-COR 926-
564 32213) and visualised by infrared fluorescence (ODYSSEY CLx, LI-COR). Average
565 phosphorylation signal was calculated using densitometry (ImageJ v 1.48).

566 **Isolation of tonoplasts and Western blotting**

567 Five plants at the rosette stage were coated using a paint brush with tween 0.05%, cycloheximide
568 (CHX) 50 µM or chlorpromazine (CPZ) 50 µM in tween 0.05%, one hour before being sprayed
569 with ABA (100 µM) or with a mock solution (tween 0.05%). One hour after ABA treatment, the
570 samples were frozen in liquid nitrogen and ground using a mortar and a pestle. Microsomes were
571 extracted according to Lund and Fuglsang [37] with an altered homogenisation buffer according to
572 Rea, et al. [38]. Briefly, ground material was extracted in 1.1 M glycerol, 5 mM Tris-EDTA, 5 mM
573 DTT, 1% [w/v] PVP-40, 1 mM PMSF, 70 mM Tris-Mes [pH 8.0] and centrifuged at 6,000g for 10
574 min. The pellet was resuspended in 3.5 mL buffer 330/5 (0.33 M sucrose, 5 mM potassium
575 phosphate pH 7.8) using a glass homogenizer. Three grams of microsomal fraction was added on
576 top of 9 g polymer solution (3.72 g of 20% Dextran T500 solution, 1.86 g of 40% PEG4000 solution,
577 1.08 g sucrose, 225 µL potassium phosphate buffer 0.2 M pH 7.8, 18 µL KCl 2 M, H₂O up to 9 g).
578 In parallel, a blank tube was made with 3 g of buffer 330/5 that was added on top of the polymer
579 solution. The tubes were gently inverted 12 times and centrifuged at 1,000g for 5 min. The lower
580 phase enriched in tonoplast was collected and re-purified using the top phase of the blank tube. The
581 bottom phase was collected and diluted 10 times with buffer 300/5. The tonoplasts were centrifuged
582 at 100,000g for 60 min. The lower phase enriched in tonoplast was resuspended in 0.1 ml RIPA
583 buffer (Fisher scientific, Nottingham, UK) and loaded onto a 4-12% SDS-PAGE NuPAGE™
584 (Thermofisher, UK). The western blotting was performed according to Pijacka, et al. [32]. Briefly,
585 an Amersham ECL Plex Western blotting system was used on which the gel was run for 2 hours at
586 120V and protein was subsequently transferred onto a low-fluorescent PVDF membrane (GE
587 Healthcare, Buckinghamshire, UK) using NuPAGE Transfer Buffer (Thermofisher, UK) for 1 hour
588 at 30V in a mini gel tank (Thermofisher, UK). The membrane was cut horizontally in two parts,

589 with the upper part incubated overnight at 4°C with anti-GFP antibody (at 1:2000 dilution) and the
590 bottom part with anti TIP1-1 antibody (at 1:5000 dilution), ensuring equal protein ratio between
591 lanes. Fluorescent secondary antibodies were incubated for one hour and the blots were imaged
592 using fluorescent laser scanner (Typhoon, GE Healthcare, Buckinghamshire, UK). Quantification
593 of bands was performed using CLIQS software (Totallab, Newcastle upon Tyne, UK).

594 To determine change in tonoplast expression in response to ABA or CO₂, plants were treated for up
595 to 2h with 50 μM ABA or 1000 ppm CO₂. Immunoblotting was carried out as described above and
596 relative expression levels were determined using TIP1;1 as marker and ImageJ [31] software to
597 quantify band intensities.

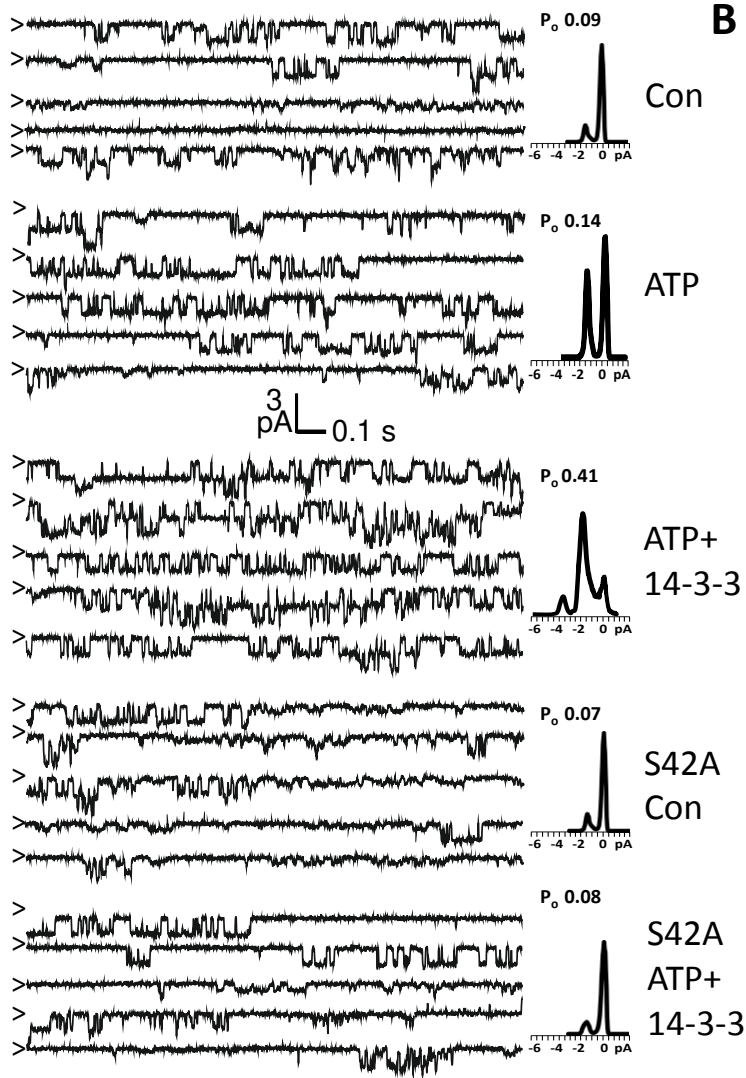
598 **QUANTIFICATION AND STATISTICAL ANALYSIS**

599 Where statistical testing of data was applied, it is indicated in the legend of the respective figure, as
600 is the number ('n') of experimental replicates. For ANOVA analyses, Prism 6 (Graphpad software)
601 was used. If ANOVA revealed significant ($p < 0.05$) effect of group, post hoc test used to determine
602 p values for all relevant comparisons is mentioned in the figure legends.

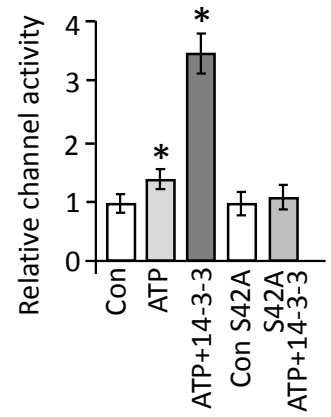
603 **Data S1 'Patch clamp open probabilities' (related to Figures 1E and S2A).** The spreadsheet
604 shows open probabilities for each kinase genotype in control, plus ATP or plus ATP+14-3-3
605 conditions.

Figure 1

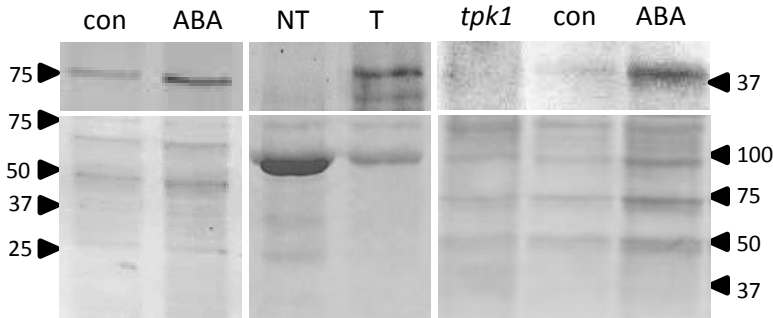
A



B



C



D



E

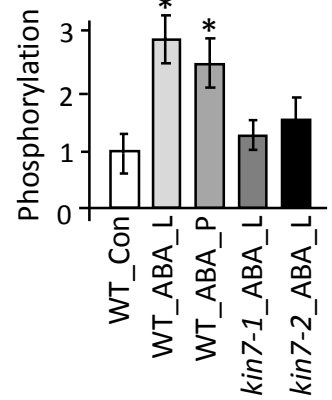
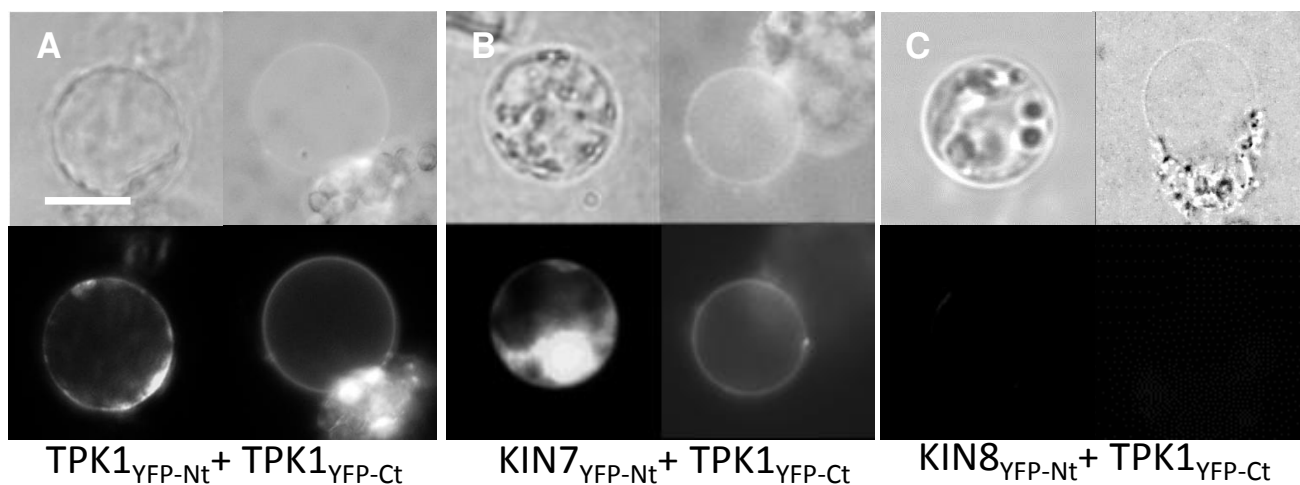


Figure 2



TPK1_{YFP-Nt}+TPK1_{YFP-Ct}

KIN7_{YFP-Nt}+TPK1_{YFP-Ct}

KIN8_{YFP-Nt}+TPK1_{YFP-Ct}

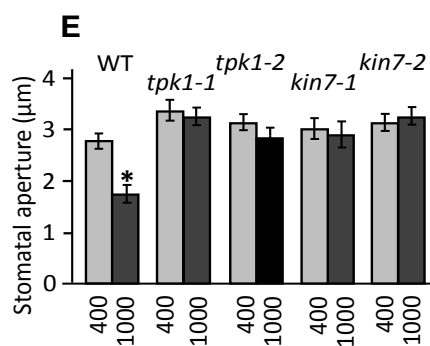
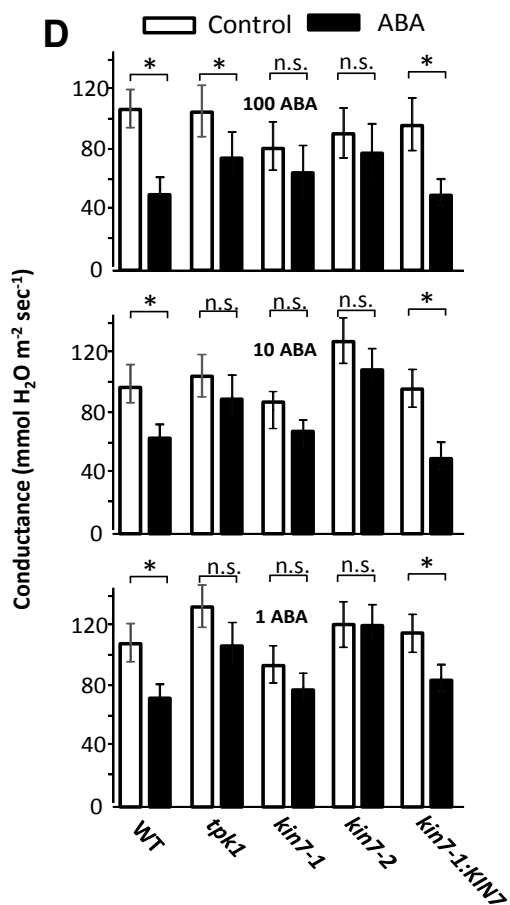


Figure3

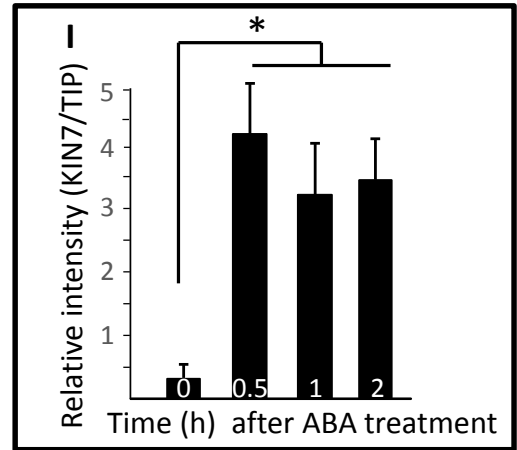
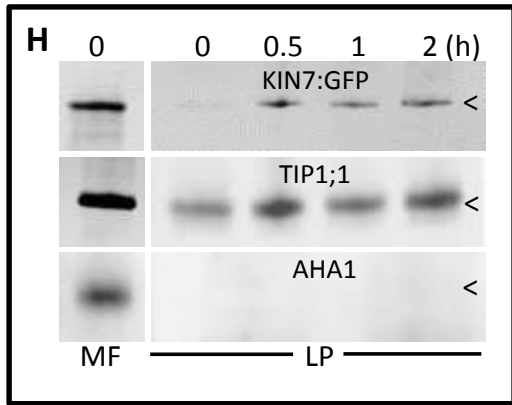
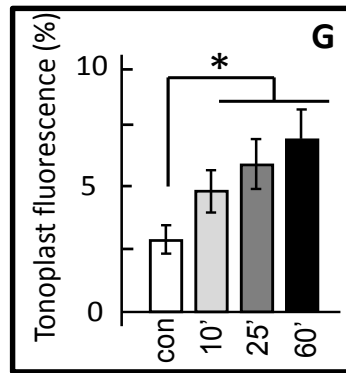
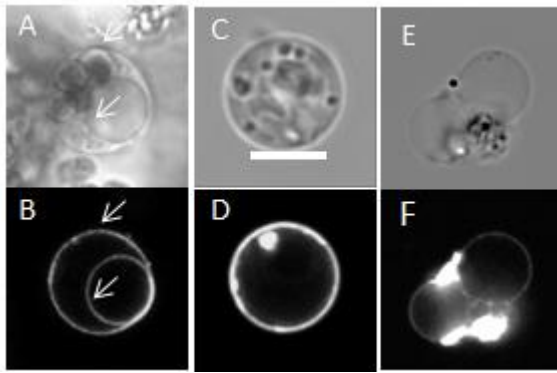
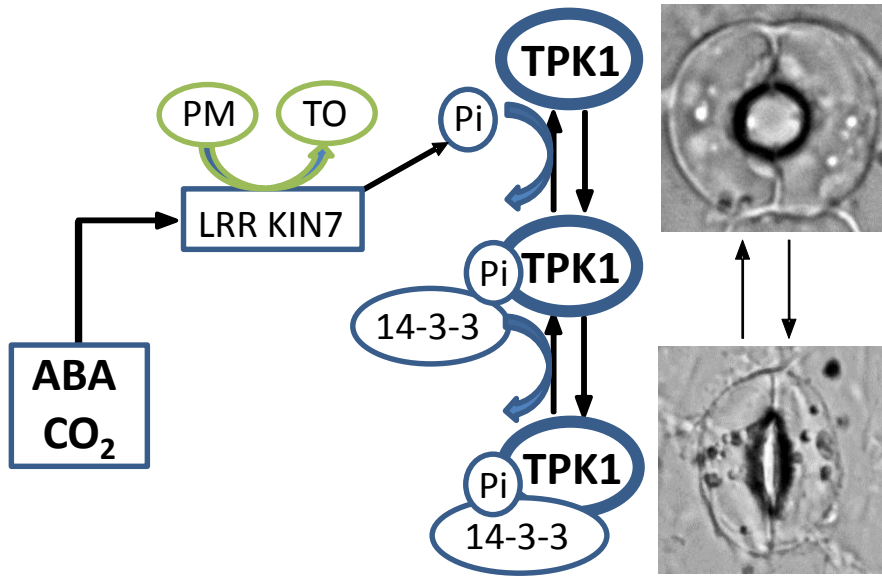


Figure4



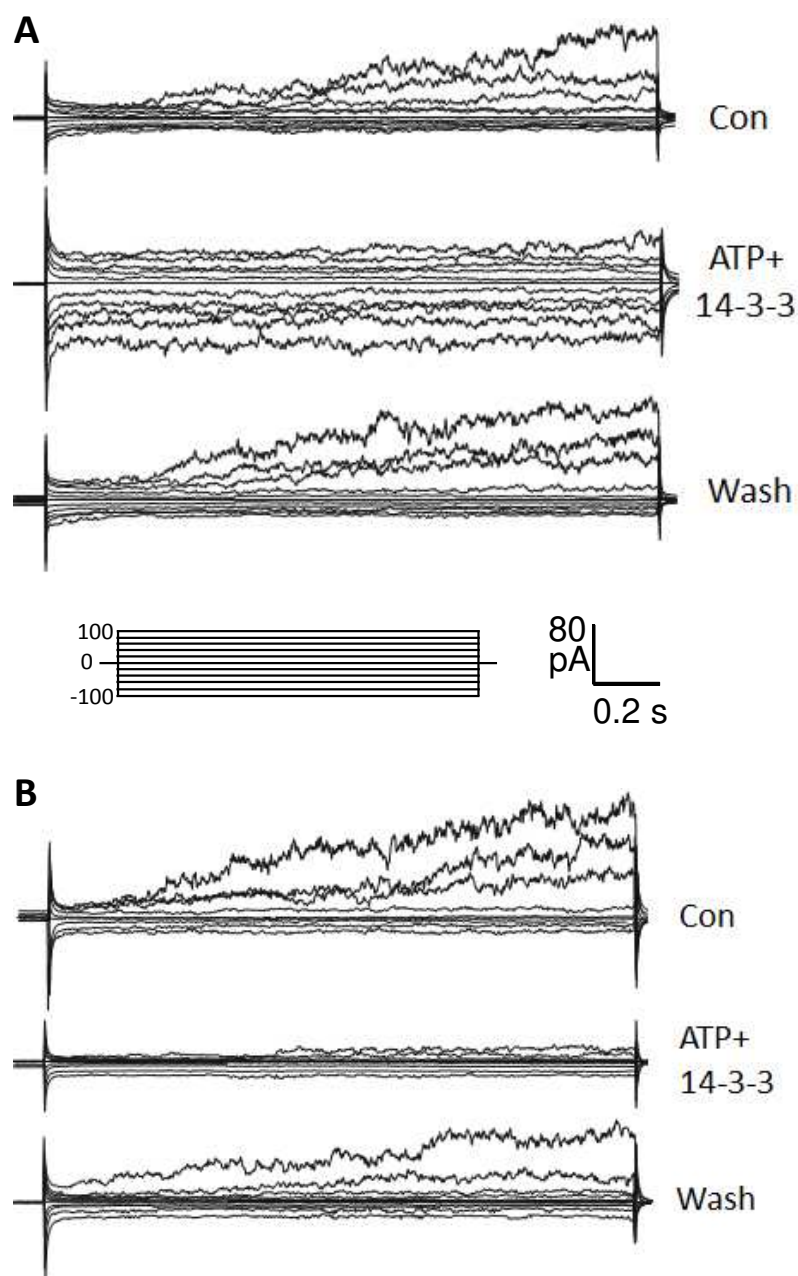


Figure S1: Whole vacuole currents (relating to Figure 1).

(A), WT guard cell whole vacuole currents in standard buffer, after exposure to buffer containing ATP+14-3-3 and after washout of ATP and 14-3-3. **(B)** Same protocol as shown in (A) for a vacuole that expresses TPK1 with the S42A mutation. Note voltage dependent activation of the SV-type current at positive voltages in control conditions and its inhibition by 14-3-3. Also note absence of TPK1 current activation in the S42A mutant. Inset shows applied voltage clamp protocol (-100 to 100 mV).

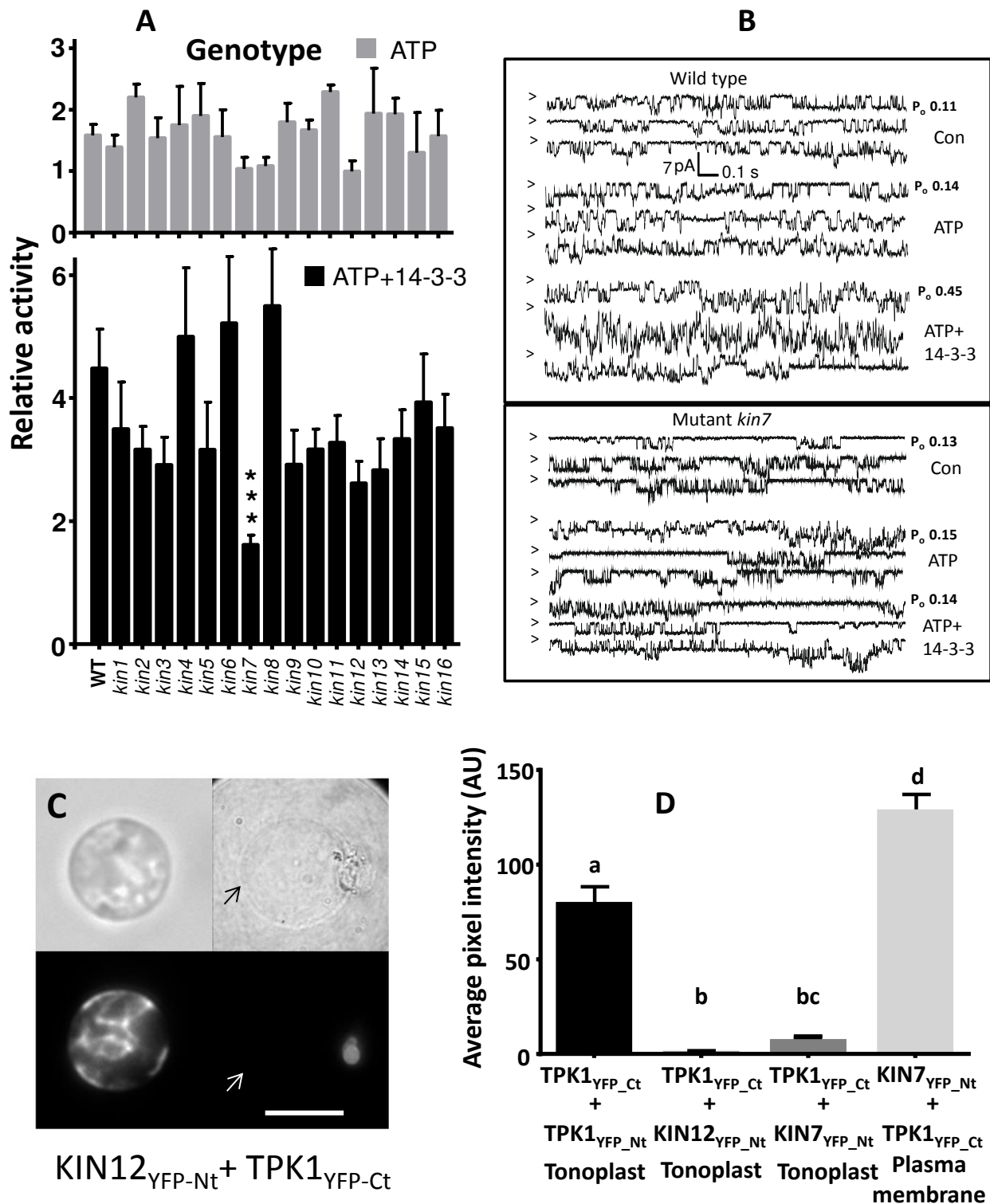


Figure S2: Kin mutant currents and BiFC (relating to Figure 2).

(A) Vacuolar cytoplasmic side out patches (n=5 to 10), isolated from wild type plants and from 16 different kinase loss of function mutants were recorded in control buffer, in the presence of MgATP, and MgATP plus 14-3-3 protein. Channel activity in the presence of ATP (or ATP+14-3-3) was compared to that measured in the control solution. The ratios of activities between ATP (or ATP+14-3-3) and control solution were then used for analysis. Data show the average for each genotype +/- SEM. The *kin7* genotype stimulatory effect of 14-3-3 (bottom panel) was significantly lowered compared to the WT. Data were tested using

a one-way ANOVA with Dunnett post hoc test analysis *** $p < 0.001$. **(B)** Example traces that reflect the different levels of current stimulation by ATP and by ATP+14-3-3 for wild type, and *kin7* KO mutants. **(C)** BiFC fluorescence in guard cell cotransformed with KIN12_{YFP-Nt} and TPK1_{YFP-CT}. Top two panels show DIC images of intact and osmotically ruptured protoplast. Bottom panels show corresponding fluorescence signal. Scale bar is 10 μm . **(D)** Quantification of BiFC fluorescence signals. Data were analysed using one way ANOVA with Tukey post-hoc analysis, different letters denoting $p < 0.05$.

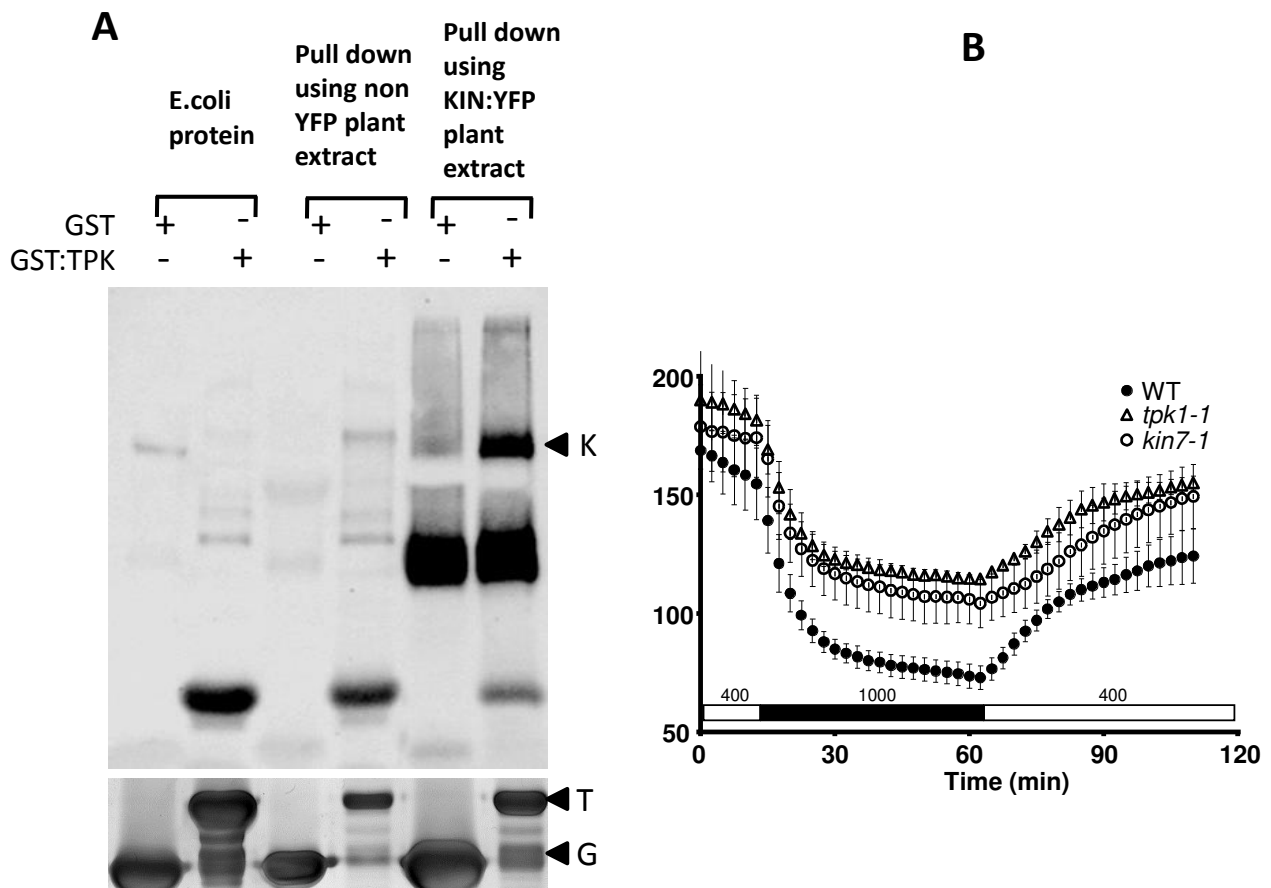


Figure S3: Pull-down assays and stomatal conductance in response to elevated CO₂ (relating to Figure 2).

(A) Pull down assays were carried out using the N-terminal part of TPK1 fused to GST as bait (or GST alone) and leaf extract from wild type plants or plants expressing KIN7::YFP as bait. A primary anti-GFP antibody and HRP-coupled secondary antibody were used to visualise bands on the blot. Arrow head on the top panel (K) depicts 100 kDa (expected KIN7::YFP size ~95 kDa), bottom panel G for GST (~26 kDa) and T for GST:TPK1 (~37 kDa). The top panel represents immunoblot using anti-GFP antibody and the bottom panel represents the corresponding gel stained using Coomassie. **(B)** Leaf conductance time courses (n=3 leaves per genotype) in response to changing ambient CO₂ which is 400 ppm for the first 10 minutes, raised to 1000 ppm for one hour and brought back to 400 ppm for another hour. Note the unresponsiveness for both the *tpk1* and *kin7* loss of function mutants.

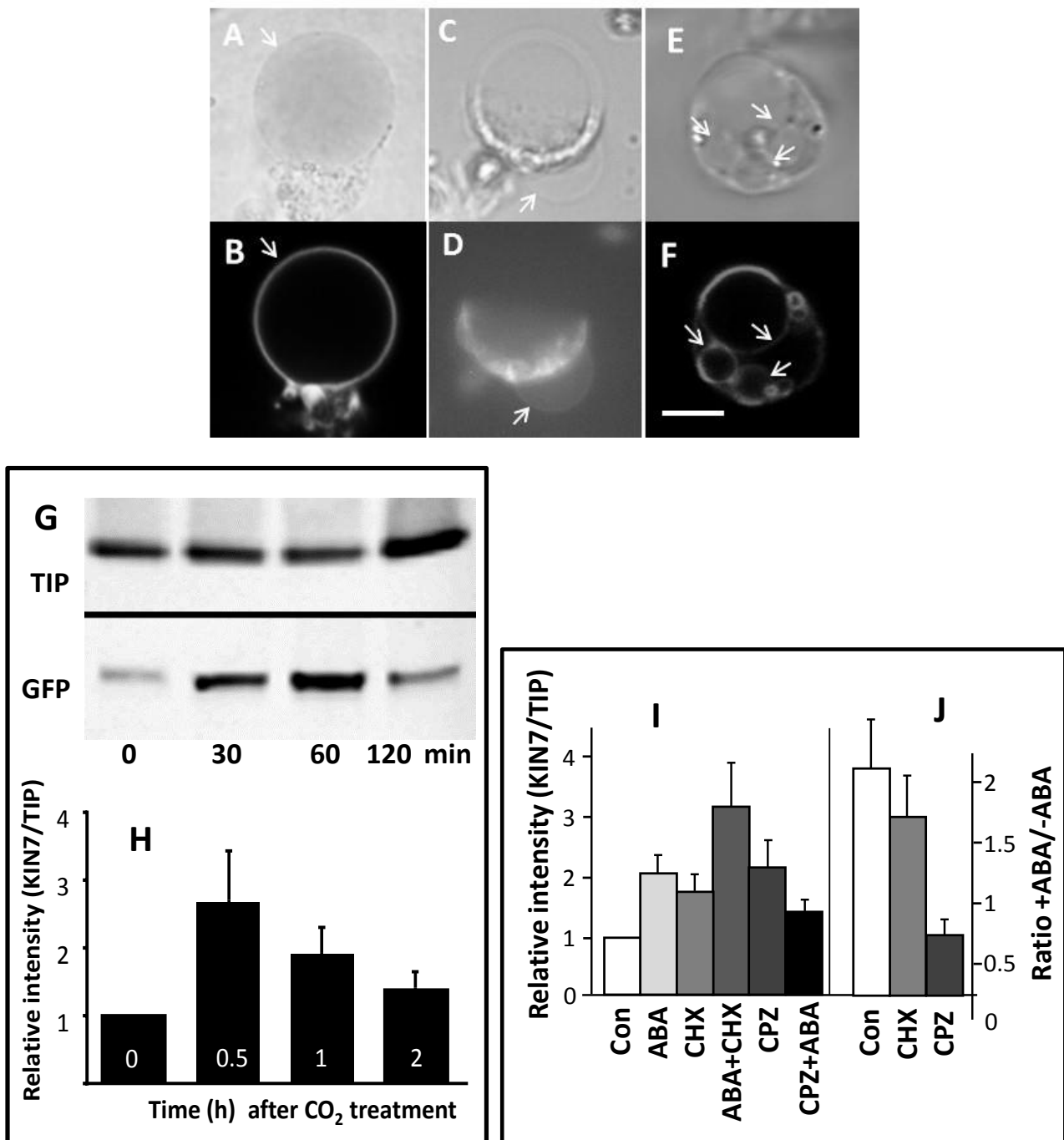


Figure S4: KIN7-YFP membrane expression pattern, CO₂ induced shift in expression and the effect of protein synthesis and endocytosis inhibitors (relating to Figure 3). (A, B) Arabidopsis guard cells transiently transformed with 35S:KIN7-YFP show KIN7 expression in tonoplast (white arrows). (C, D) Partially disrupted guard cell protoplast transiently transformed with Kin7p:KIN7-YFP shows fluorescence in large vacuolar bulge (arrows). (E, F), Guard cell protoplasts isolated from plants stably transformed with Kin7p:KIN7-YFP shows fluorescence large and multiple small vacuoles (arrows). Top row shows DIC images, bottom row shows corresponding epifluorescence images. Scale bar is 3 μ m. (G) Example Western blot using antibodies against KIN7-GFP and TIP1;1, showing that CO₂ treatment (1000 ppm, 3h) causes an increase in KIN7 expression relative to TIP1;1, a marker for the tonoplast. (H) Data were quantified on the basis of 3 independent biological replicates, error bars denote standard errors. (I) Treatment of plants with ABA,

cycloheximide (CHX, a protein synthesis inhibitor) or chlorpromazine (CPZ, an inhibitor of endocytosis) on their own, causes a shift in KIN7 expression towards tonoplast location. Cycloheximide and chlorpromazine stimulate an increased KIN7:TIP ratio when used on their own, pointing to non-specific effects of these inhibitors. The effect of ABA is abrogated in plants pre-treated with chlorpromazine. This becomes obvious when plus/minus ABA ratios are compared for the various treatments (Figure 3B). **(J)** Same data as in (A) but expressed as a ratio of plus ABA to minus ABA treatment. This shows that cycloheximide does not affect the ABA-dependent shift toward tonoplast expression whereas chlorpromazine strongly inhibits it. Data are from 3 independent experiments and error bars denote standard errors.

KIN#	Gene ID	Annotation	Mutant line	TMD
1	AT1G21250	WAK1, wall associated kinase	SALK_209668	1
2	AT1G48480	RKL1 (Receptor-like kinase 1)	SALK_099094	2
3	AT1G51805	Leucine-rich repeat protein kinase,	SALK_003231	1
4	AT1G53730	SRF6 (Strubbelig-receptor family 6)	SALK_054337	2
5	AT1G66150	TMK1 (Transmembrane kinase 1)	SALK_008771	1
6	AT2G26730	Leucine-rich repeat transmembrane protein kinase	SALK_034004	1
7	AT3G02880	Leucine-rich repeat transmembrane protein kinase	SALK_019840/FLAG_321B08	1
8	AT3G14840	Leucine-rich repeat family protein	SALK_094512	2
9	AT3G22060	Receptor protein kinase-related	SALK_151902	1
10	AT4G01330	Protein kinase family protein	SALK_081284	1
11	AT4G21380	ARK3 (<i>Arabidopsis</i> Receptor Kinase 3)	SALK_001986	2
12	AT4G21410	Protein kinase family protein (CRK29)	SAIL_447_F06	1
13	AT4G29130	AtHXK1 (GLUCOSE INSENSITIVE 2) hexokinase	SALK_018086	1
14	AT4G34220	Leucine-rich repeat transmembrane protein kinase	SALK_112336	2
15	AT5G38990	Protein kinase family protein	SALK_139579	1
16	AT5G49760	Leucine-rich repeat family protein kinase	SALK_118908	2

Table S1: Vacuolar kinases (related to Figure 1, Table S2 and Figure S2).

Membrane kinases identified in the SUBA database (suba2.plantenergy.uwa.edu.au/) with a 'vacuolar' localisation based on either 'GFP' or MS/MS analyses. 'TMD': putative number of transmembrane domains. For each, loss of function mutants were obtained which were genotyped using T-DNA and gene specific primers (see Table S2). RT-PCR on RNA from homozygous lines was carried out, using gene specific primers, to ensure no transcript was present.

Mutant Line	Forward and Reverse genotyping primers
SALK_209668	5'AATCTGCGAAATGTCATGAGG3' 5'TTGGTATCAGCCTTGAAGCAC3'
SALK_099094	5'TCTCTGTTTTCTCTCCCTCC3' 5'GTCAAGCACTGCCTTATACGC3'
SALK_003231	5'TTCTTACATGACAAAAATTCAGGG3' 5'AGCTCAAGATCAACCCGGTAC3'
SALK_054337	5'AACGACTTTCACGGTATGCAC3' 5'TGTCAAATGGTTTTCTCCCAG3'
SALK_008771	5'CGAGAAAACCGGGTAAAGAAC3' 5'TTTTTGTGCGAATAAACAACCTTG3'
SALK_034004	5'GCCACCAGATAAATATTTGC3' 5'AGTGAGTCGACCTAAGGAGCC3'
SALK_019840	5'CATGAAAACAAAGGGATGAGG3' 5'CACGCAGAGGATATCGAGAAG3'
GABI_047F11	5'TAAATGGTTTAAGCGGTGTGC3' 5'ATCAGCAACGGACATTTCAAC3'
FLAG_321B08	5'TATTCCGAGTTCGTTGTGTCGTC3' 5'GGAAACGGGAGAACTCCGTT3'
SALK_094512	5'CATCGATCATGCCATAAATCC3' 5'GAGCAGTTACAAGTAACGGCG3'
SALK_151902	5'TTTACCGTCGCAACAGTTAGG3' 5'TTAAACGCATCGTTTGGTTC3'
SALK_081284	5'TTCGTCTCGATATGGACAAGG3' 5'GACGACCCAAAGCTTTAGACC3'
SALK_001986	5'TCAAAGACATCAGTTCAGGGG3' 5'TTCACTGTCCATGATTCATCG3'
SAIL_447F06	5'TCTCAGCATCACAACAACCTCG3' 5'AAATACAGCAGGAGGGATGTG3'
SALK_018086	5'CTCGAAACTGAGACAAGTGGC3' 5'GTCTTCGCATTCTGTAGCGAC3'
SALK_112336	5'CTCGAAACTGAGACAAGTGGC3' 5'GTCTTCGCATTCTGTAGCGAC3'
SALK_139579	5'CTCTCGAATTCCTTGGGTTTC3' 5'CAATCTCTCTGGTGATTTGCC3'
SALK_118908	5'TCAATGGACGTAACTTTGAGG3' 5'AGTGAAACGGTTGACGTTGAC3'
	Cloning primers
kin8bifcfwd	CCACTAGTGGAAACAATGTCGTTAAATCGACAACCTTCT
kin8bifcrev	CGACTCGAGAGTTCTAGTGTTC CAATAGG
kin12bifcfwd	CCGGATCCGGAACAATGGAACATGTCAGAGTTATCT
kin12bifcrev	CGACTCGAGACGAGGAGAAAACCTCAGAAA
kin7bifcfwd	CCACTAGTGGAAACAATGAAGTATAAGCGTAAGCT
kin7bifcrev	CGACTCGAGGTCGGATACAGGATTTGGGG
tpk1bamhlf	GGATCCATGTGAGTGATGCAGCT
tpk1xhoir	CTCGAGCTACATGATCACTCGCCTGAG
kin7yfpfwd	CGACTCGAGAACAATGAAGTATAAGCGTAAGCT
promkin7fwd	ATGTCTTTGGTCACACTCAACCTGC
promkin7rev	CACTCGAGCTTCTTCTTCTTCTTCAAAAAC
kin7yfpfwd	CGACTCGAGAACAATGAAGTATAAGCGTAAGCT
kin7yfprev	ACCCGGGGTTCGGATACAGGATTTGGGG

Table S2: Genotyping and cloning primers (related to Star Method section 'Plants' and 'Cloning of kinases in the BiFC vector').

Gene specific primers used to identify homozygous lines for kinase mutant lines listed in Table S1 and cloning primers used to make kinase-YFP fusion proteins.